

# Design of properties and performances of innovative gas diffusion media for polymer electrolyte membrane fuel cells

Saverio Latorrata <sup>a,\*</sup>, Riccardo Balzarotti <sup>a</sup>, Paola Gallo Stampino <sup>a</sup>, Cinzia Cristiani <sup>a</sup>, Giovanni Dotelli <sup>a</sup>,  
Manfredo Guilizzoni <sup>b</sup>

<sup>a</sup> Politecnico di Milano, Dipartimento di Chimica, Materiali e Ingegneria Chimica "G. Natta", Piazza Leonardo da Vinci 32, 20133 Milano, Italy

<sup>b</sup> Politecnico di Milano, Dipartimento di Energia, Via Lambruschini 4, 20156 Milano, Italy

## 1. Introduction

Polymer electrolyte membrane fuel cells (PEMFCs) are electrochemical devices that produce electricity through the direct electrochemical oxidation of a fuel (usually hydrogen) and the reduction of oxygen with high efficiency and low environmental impact. Moreover, PEMFCs are capable of producing high power densities and undergoing rapid changes in load; thus, they are regarded an alternative power source for both automotive and stationary applications [1–5].

PEMFCs performances and costs mainly depend on the membrane electrode assembly (MEA), composed by the polymer electrolyte membrane and the two catalytic layers (i.e. anode and cathode). Between the MEA and bipolar plate, where serpentine with the flow field lie, the so-called gas diffusion medium (GDM), fundamental to the proper working of the fuel cell (FC), is inserted. It plays an important role in determining the electrochemical performance of the device since it has to guarantee a proper transport

of water. An efficient water management is a key factor to obtain enough power, to prevent degradation of materials and to avoid flooding of the electrodes during operation of a PEMFC. Indeed both deficiency and excess water would cause severe problems to power generation. Water deficiency would result in reduction of ionic conductivity of the membrane as well as it would drive to severe contact resistances between the membrane and the catalyst layer; on the other hand, excess water would cause diffusive limitations thus reducing catalytic sites for electrochemical reactions and hindering reactants transport to the electrodes [6–10]. It has been demonstrated that GDM is able to manage water efficiently depending on composition and properties such as thickness, porosity, hydrophobicity and permeability [11]. An optimal GDM reduces flooding under high relative humidity (RH) conditions and prevents membrane dehydration under low RH conditions [10,12–14].

GDM consists of two main components, a gas diffusion layer (GDL), which can be a macro-porous carbon-fibre, carbon-cloth or woven-non-woven substrate and a micro-porous layer (MPL) which is a carbon layer.

Gas diffusion layer (GDL) can remove reaction products (exhausted gases and water) from the catalyst layer and it can favour heat removal from the MEA. Moreover, it can guarantee

\* Corresponding author. Tel.: +39 02 23993233; fax: +39 02 70638173.  
E-mail address: [saverio.latorrata@polimi.it](mailto:saverio.latorrata@polimi.it) (S. Latorrata).

a good contact between bipolar plates and MEA. In this respect, GDL characteristics, such as electronic and thermal conductivity, porosity, hydrophobicity, compressibility and elasticity, play a crucial role in determining the water management efficiency during PEMFC operations [9,15–18]. MPL is directly coated onto GDL surface and it consists of carbon particles and of a hydrophobic agent, namely PTFE. Due to its micro-porosity it improves capillary pressure, thus the water removal capability. Many studies have demonstrated that a MPL coated onto the GDL is effective in improving water management, thereby getting better electrical performances [7,9,10,12,14,16,19,20].

A more hydrophobic MPL would allow a faster water removal process at the cathode side [21]. A typical MPL formulation mainly contains carbon black (CB), polytetrafluoroethylene (PTFE), both as binder and hydrophobic agent. CB is dispersed using proper solvents and dispersants, then a PTFE suspension is added. The resulting ink is deposited onto one side of the GDL substrate pre-treated with PTFE. A subsequent thermal treatment of the formed GDM is required to evaporate the solvent and the surfactant and to induce the polymer spreading onto the carbon, called in the literature sintering [11].

The effect on water management of the different MPL components has been extensively investigated during the last decade [9,11]. Nature and loading of the carbon powder, wettability, thickness and porosity of the layer surface were suggested to be responsible for the final MPL properties. Much less attention has been paid on the nature of the hydrophobic agent, keeping PTFE as the best choice for that purpose for many years. Only few works have dealt with the use of different polymers such as fluorinated ethylene propylene (FEP) [22,23] and polyvinylidene fluoride (PVDF) [24–27].

Some of us have recently reported the beneficial effects of the use of perfluoropolyether derivatives for hydrophobic surface treatments of GDLs [28].

In the present study, three different fluorinated polymers were tested in order to replace PTFE: perfluoroalcoxy (Teflon® PFA), fluorinated ethylene propylene (Teflon® FEP) and a fluorinated polyurethane (Fluorolink® P56, Solvay) based on perfluoropolyether (PFPE) blocks [29–33] were applied to make both GDLs (i.e. the substrate) and MPLs (i.e. the coated layer) hydrophobic.

Different formulations were prepared and the effect of the polymers nature on the rheological behaviour of the ink was studied in order to apply doctor blade technique for coating deposition. The influence of the polymer nature on the final GDLs and MPLs properties, such as contact angle values and morphology, was studied with the final target to evidence a relationship between GDM composition and electrochemical behaviour of the running fuel cell.

## 2. Experimental

### 2.1. Preparation

Commercial carbon cloths (S5, from SAATI, Italy) were used as GDLs.

Commercial aqueous dispersions of polymers as hydrophobic agents were used for polymers raw materials: a high molecular perfluoropolyether (PFPE) Fluorolink® P56 from Solvay Solexis, fluorinated ethylene propylene (FEP) and perfluoroalcoxy (PFA) both from DuPont.

Before coating deposition, the surfaces of the bare GDLs were hydrophobized by soaking in a solution of the selected fluorinated polymer for 20 min. Subsequently they were heated in air for 30 min up to 150 °C, 260 °C and 305 °C to melt and to make PFPE, FEP and PFA fibrous, respectively [34].

**Table 1**

Inks composition in terms of significant ratios. Ink based on PTFE refers to sample prepared in [13] in which surfactant was Triton X-100.

Sample name	CB/H <sub>2</sub> O (w/w)	Polymer/CB (w/w)	CB/IPA (w/w)	CB/Triton (w/w)
ink-PTFE	0.13	0.12	–	5.6
ink-PFA	0.13	0.12	5.6	–
ink-FEP	0.13	0.12	5.6	–
ink-PFPE	–	0.12	7.72	–

Highly conductive graphitic carbon black (CB, Cabot Vulcan XC72R) with high surface area was used for MPL preparation. Isopropyl alcohol (IPA), supplied by Sigma–Aldrich, was used as solvent and dispersant. Slurry composition and experimental procedures were selected according to a procedure previously reported [13].

In a typical experiment, CB was slowly added to a solution of the polymer dispersion and IPA (Triton X-100 in the reference ink preparation based on PTFE [13]) in deionized water. The mixture was vigorously stirred and homogenized by a high shear mixer (UltraTurrax T25) at 8000 rpm for 10 min.

The final inks compositions are reported in Table 1; the selected formulation would guarantee a proper rheological behaviour of the ink when used in blade coating procedure.

Indeed, the obtained inks were deposited onto the hydrophobized GDL substrate via the blade coating technique, using a lab-scale commercial equipment K-101 Control Coater. A linear velocity of 0.0154 m/s and a 40 μm gap, corresponding to a shear rate of about 350 s<sup>-1</sup>, were adopted.

Finally, to remove water and IPA and to sinter the fluorinated polymer, the coated samples were heated in air up to 150 °C, 260 °C and 305 °C (30 min) for PFPE, FEP and PFA, respectively. Reference samples based on PTFE were treated at 350 °C [13].

### 2.2. Characterization

X-ray diffraction (XRD) analysis of the fluorinated polymers was performed using a Bruker–D8 Advance instrument. Spectra were recorded under the following experimental conditions: Cu Kα radiation, 2θ range = 20–80° 2θ, step scan = 0.02° and time per step = 12 s. The crystallinity degree was estimated by XRD pattern using the following equation:

$$x_c = \frac{I_c}{I_c + I_a}$$

where  $I_c$  is the diffracted intensity of the crystalline peak at about 18° 2θ and  $I_a$  is the diffracted intensity of the amorphous halo at about 16° 2θ.

DSC thermograms of the fluorinated polymers were recorded in air using a Mettler Toledo 823e instrument, temperature range: r.t. – 400 °C and heating and cooling rates 10 °C/min.

The rheological behaviour of the inks was tested at 20 °C by means of a rotational rheometer (Rheometrics DFR 200) equipped with a 40 mm parallel-plates geometry, with a gap between the stationary plate and the movable one of 1 mm. Dynamic viscosities were investigated in the shear rates range 10<sup>-3</sup> to 10<sup>3</sup> s<sup>-1</sup>.

Contact angles were measured with a modified axisymmetric drop shape analysis technique [35] using “as placed” sessile drops [36], i.e. gently deposited drops on a fixed surface with no vibration or other disturbances. A high precision metering pump with suitable syringes was used to generate drops of controlled volume and side views of such drops were taken using a diffuse 800 W light and a SLR digital camera with a 60 mm F2.8 Macro-lens. The side shot of the deposited drop were processed with the technique described in [37,38]: the numerical integration of the axisymmetric Laplace–Young equation in dimensionless arc-length coordinates was fitted

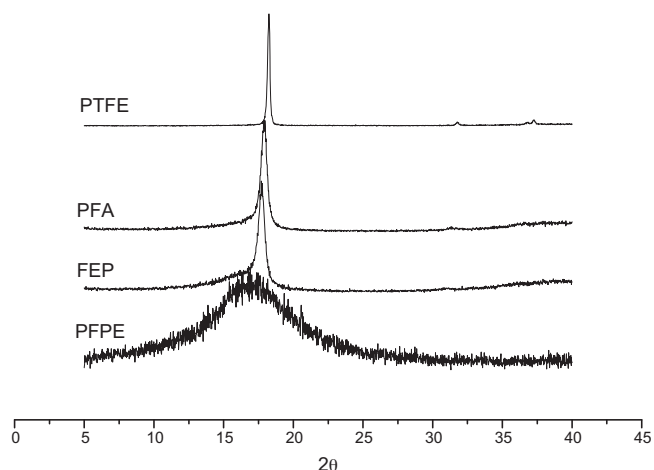


Fig. 1. Results of XRD analysis of the four polymers employed.

to the experimental drop contour. A “selected plane” approach [39], using the drop maximum diameter, was used to get a starting value of the drop Eötvös number; then a fitting (in a least square sense) to the experimental drop contour was performed to get the final fitted profile. The contact angle was finally determined as the value of the tangential angle to such profile at the intersection between the latter and the experimentally detected baseline. As the surfaces are rough, such angle has to be understood as an apparent contact angle.

A Cambridge Stereoscan 360 scanning electron microscope (SEM) was used for the morphological analyses of GDMs. SEM analyses were carried out both onto the surfaces and the cross sections of the samples, that were gold coated to prevent charging effects.

The pore diameter, pore size distribution and pore volume/porosity of the prepared GDMs after thermal treatment were measured by the mercury intrusion technique using a Carlo Erba Porosimeter 2000 Series instrument. The pore size distributions were calculated by applying the Washburn equation.

To verify the influence of the polymer nature on the final electrical performances, the GDMs were tested in a single lab-scale cell in terms of polarization, power density curves and electrochemical impedance spectroscopy (EIS) at 60 °C and 80 °C and relative humidity 80–100% (anode–cathode). Graphitic bipolar plates, with a single serpentine at the anode and a triple one at the cathode, were used. A commercial Nafion-based catalyst coated membrane (CCM, supplied by Baltic fuel cells) was employed as MEA. The platinum loading was 0.3 mg cm<sup>-2</sup> at the anode and 0.6 mg cm<sup>-2</sup> at the cathode. Hydrogen (0.2 NL/min) and air (1 NL/min) were the anodic and cathodic feedings, respectively. Humidity and the inlet gas temperature were controlled by external humidifiers and temperature controllers. Voltage, current and generated power were measured with an electronic load (RBL488-50-150-800) connected to the cell.

### 3. Results

#### 3.1. Polymers characterization

The XRD analysis of the different polymers is reported in Fig. 1; for the sake of comparison, XRD of PTFE is also reported. It is evident that FEP and PFA are crystalline, while PFPE is amorphous. Degree of crystallinity of about 45% and 65% was found for FEP and PFA, respectively, while almost 100% of crystallinity was found for PTFE.

The knowledge of the polymers melting temperature is basic to select the temperature of thermal treatment of the prepared GDMs and thermal treatment is fundamental to reach the final GDM properties. Indeed, it is required to eliminate the solvent and the

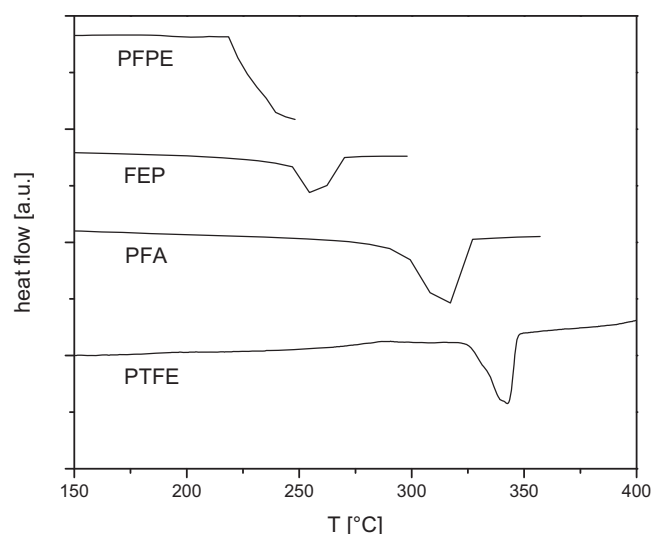


Fig. 2. Results of DSC analysis of the four polymers employed.

additives which were used for carbon dispersion, to consolidate the coated layer and finally to determine the layer porosity. On the above consideration, the final thermal treatment has to be properly tuned sample to sample on the bases of the nature of the polymer.

Accordingly, the melting points of the polymers were determined by differential scanning calorimetry (DSC) (Fig. 2). An endothermic decomposition phenomenon, is observed in the DSC analysis of the crystalline polymers, in particular it occurs at 343 °C, 307 °C, 255 °C for PTFE, PFA and FEP respectively. This peak, which corresponds to the melting point of the material, occurs at increasing temperature on increasing the degree of crystallinity of the polymer. Indeed, PFPE, that is amorphous, decomposes at 230 °C, temperature highly lower than those of the other polymers.

On the above considerations, the temperature of thermal treatment was set for each sample in correspondence of the melting phenomenon for the new polymers, while according to literature indication for PTFE [11].

#### 3.2. Rheological characterization

Pseudo-plastic shear thinning fluids are desirable for blade coating processes [40]. In Fig. 3 the flow curves of the three inks containing the new polymers are compared with that of the PTFE-based ink. Independently on the nature of the polymer, all the samples are pseudo-plastic, showing a viscosity which decreases on increasing the shear rate.

Even though the FEP curve showed scattered points at low shear rates, the three curves become very close at shear rates higher than 100 s<sup>-1</sup> (see offset of Fig. 3), typical of the blade coating technique. The rheological behaviour of similar inks compositions except for the use of PTFE has been already reported [13].

The viscosities of the inks containing the three polymers are always higher than those reported for PTFE (e.g. at shear rate 100 s<sup>-1</sup> 0.5 Pa s are found for PTFE to be compared with 2–3 Pa s for all the other fluorinated polymers). Moreover, in PTFE-containing inks the presence of some order–disorder phenomena are suggested by changes in the slope of the flow curves (see the plateau in the range of 5–10 shear rate, Fig. 3). These phenomena are less evident (smoothed plateaus are seen in the flow curves) or at least disappear when the new polymers are used in formulation, suggesting that more stable and reproducible rheological behaviours can be obtained this way.

Finally, in order to test the stability of the inks, the rheological measurements were performed not only immediately after

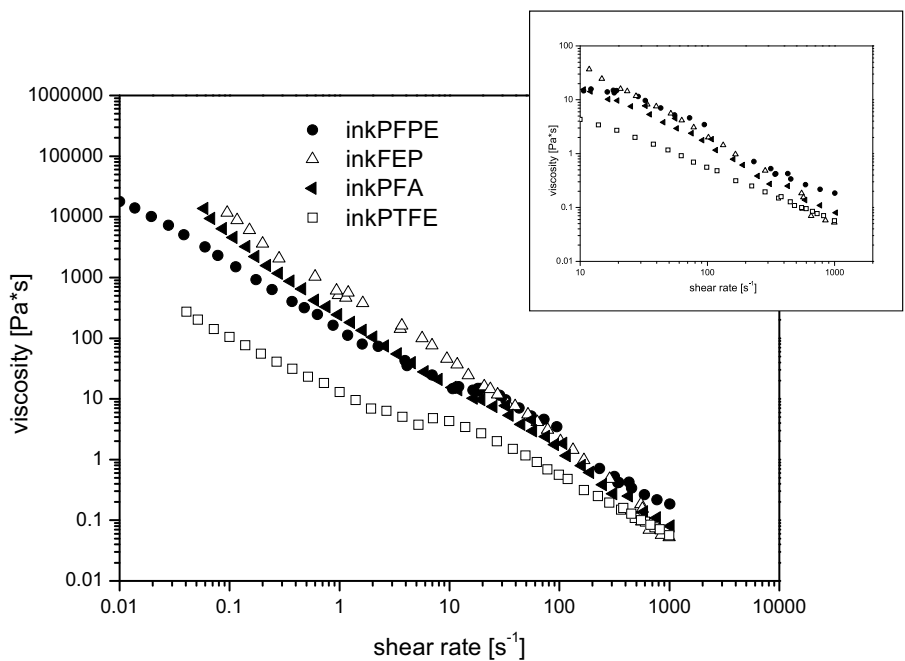


Fig. 3. Flow curves of the inks containing the different polymers.

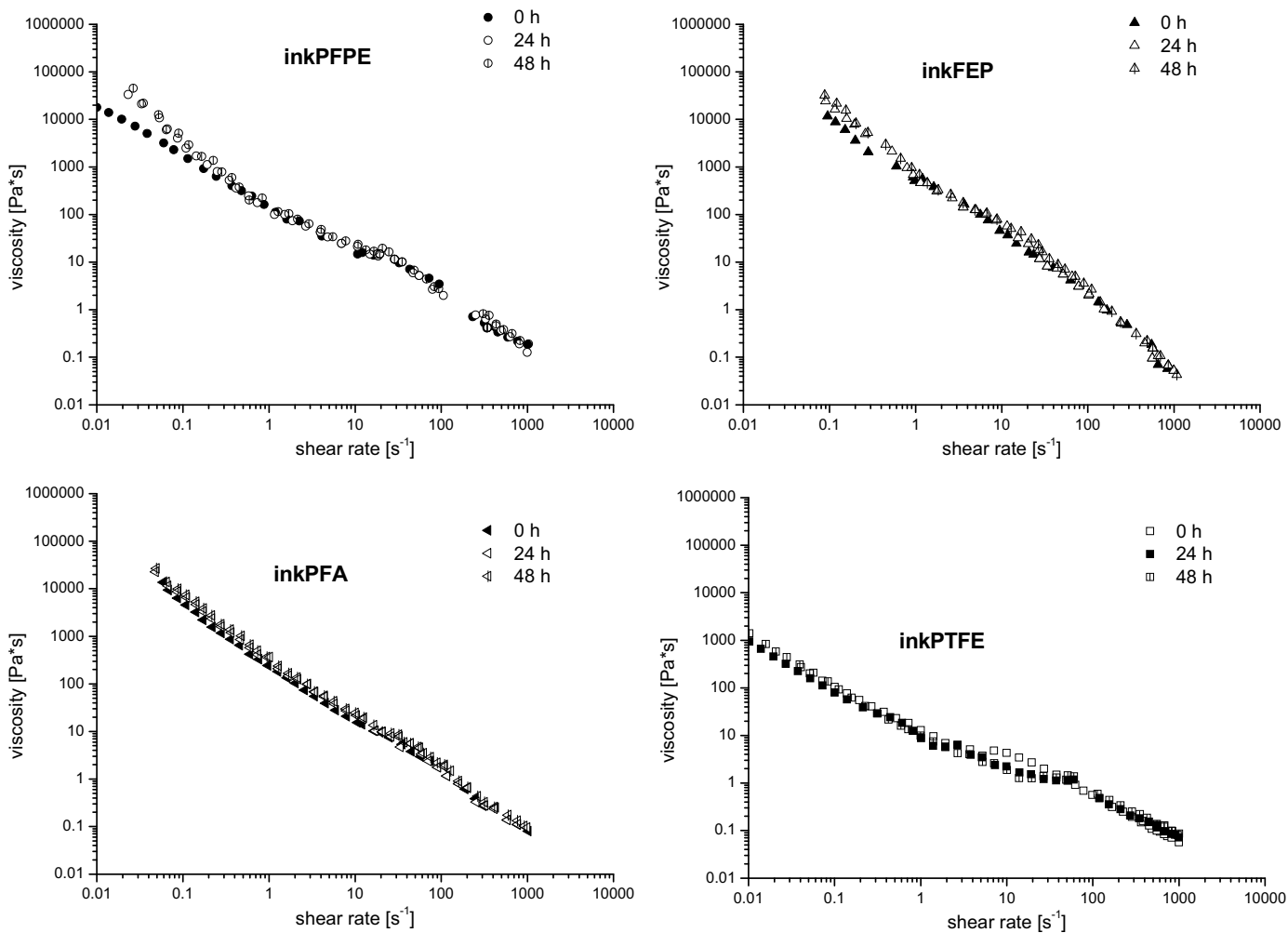


Fig. 4. Flow curves of the inks at different ageing times.

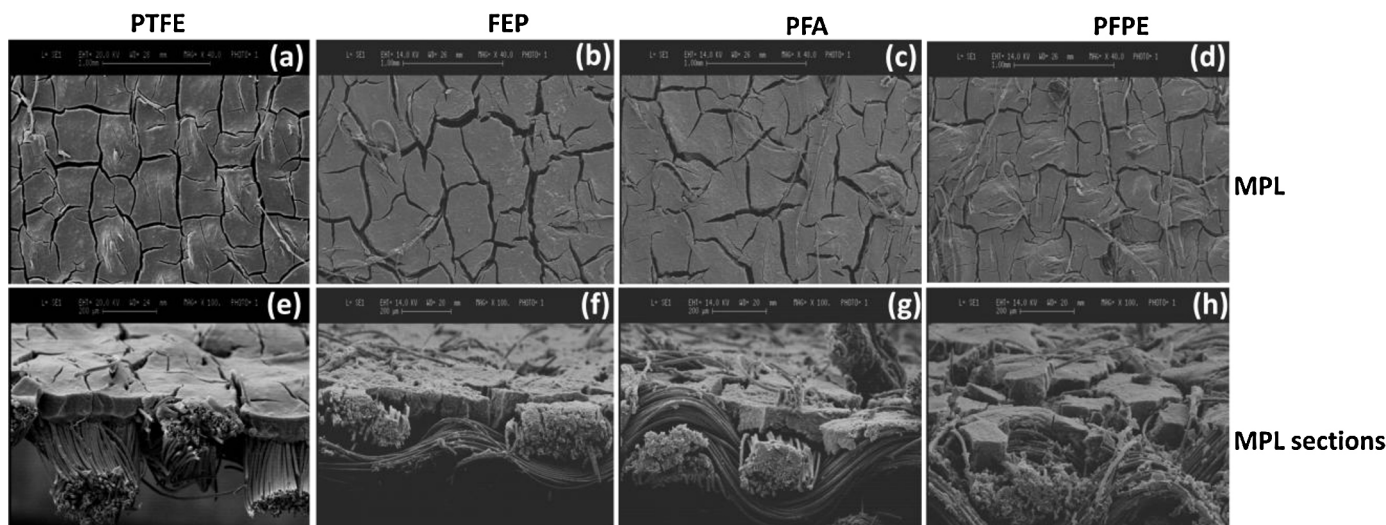


Fig. 5. SEM images of MPL surfaces (a, b, c, d, 40 $\times$ ) and MPL sections (e, f, g, h, 100 $\times$ ) of samples containing PTFE (a, e), FEP (b, f), PFA (c, g) and PFPE (d, h).

preparation, i.e.  $t = 0$  h, but also after 24 h and 48 h of ageing (Fig. 4). As observed in the case of PTFE, no remarkable effect of the ageing time is evident since the flow curves of all the inks are overlapped at the three different times. Accordingly, a good stability of the dispersion with time can be claimed similar to that of the more conventional PTFE-based slurry.

On this bases, it can be assumed that the order–disorder instability phenomena discussed above are not time-dependent, i.e. similar time stability is found in all the samples, but composition-dependent.

Bearing in mind that the layer thickness is a combination of viscosity and shear rate, it is clear that, to obtain comparable thicknesses among PFPE-, PFA-, FEP- and PTFE-based MPLs, the observed difference of viscosity has to be taken into account.

A final coating layer about 50–70  $\mu\text{m}$  thick was obtained when deposition of PTFE-containing inks was performed at shear rate of about  $100 \text{ s}^{-1}$  [13]. Accordingly, to reach the same thickness value, the deposition procedure with fluorinated polymers here studied was operated fixing the shear rate at about  $350 \text{ s}^{-1}$ .

### 3.3. Surface characterization

SEM images of the hydrophobized MPLs surface and of their section are reported in Fig. 5((a,e) PTFE, (b,f) FEP, (c,g) PFA and (d,h) PFPE). Somewhat homogeneous surfaces are evident in all the samples, suggesting that a good coverage of the GDLs was reached, even though traces of the fibres of the bare GDL are still evident, mainly in the PFPE-containing MPL. Furthermore, identifiable cracks, of variable dimensions, are found at the surface of all the samples. The presence of cracks is also reported in the literature and they are typically related to the thermal treatment process, being due to shrinkage phenomena upon solvent elimination [34].

In principle, cracks formation has to be hampered because it could result in coating shedding during the cell operation. However, if the phenomenon of cracks formation is limited to the layer surface, e.g. less deep cracks are formed, the coating detachment is negligible. Furthermore, a positive effect of the presence of slightly deep cracks has been reported [10]: since macro-pores should reduce the mass transport limitation due to water flooding, a limited number of cracks may supply alternative paths for species diffusion towards the catalytic region.

The measurement of the MPLs thicknesses is not easy, because of the very weak stiffness of the GDL substrate. However, an attempt

to evaluate thickness was performed by means of SEM cross section images: average thicknesses of 85, 50 and 65  $\mu\text{m}$  were found for GDMs prepared with FEP, PFA and PFPE, respectively. These thickness values are fairly comparable with that observed in case of PTFE-based MPL (i.e. 50–70  $\mu\text{m}$ ).

Even though only at a glance inspection, PFPE-based MPL seems to be less adherent with respect to other MPLs. This behaviour is likely due to PFPE nature, and, in particular, to the absence of a melting process since this polymer was found to be amorphous. The absence of the melting process would result in a worse consolidation of the carbon coating. In fact, the polymer traps the carbon powder particles when melted thus stabilizing the layer in a crust once cooled. Hence, the lack in polymer melting process could cause detachment of carbon particles during cell operation and result in severe issues in terms of increasing mass transfer resistance.

### 3.4. Porosimetry

Total porosities of 77%, 65%, 70% and 69% were found for GDMs containing PFPE, FEP, PFA and PTFE respectively.

Actually, the pores size dimension and distribution are also fundamental parameters of the material because, as reported in the literature [10,34,41,42], they are the most critical parameters which transport of gas and water across the GDM depends on. In particular, water transport requires the presence of both small and large pores with micro-pores which should transfer the condensed water from the condensation sites towards bipolar plates [10].

Accordingly, the pores size distribution of the four GDMs was measured and compared with that of the pristine carbon powder to evaluate the effect of the polymer nature on porosity. Results are shown in Fig. 6. Pores in the GDMs are divided (Fig. 6a) according to the size classification reported in the literature for diffusion layers for PEM fuel cells [34,43]. The distribution of the pristine carbon powder is very complex and it is quite difficult to be described in terms of pores size distribution (Fig. 6a). Except for micro-pores, a large polymodal size distribution is found. When MPLs are coated onto the GDLs surfaces, some modifications of the pores distribution occur, particularly in the meso- and micro-pores region (Fig. 6b and c). Upon MPL deposition, indeed, meso-pores are eliminated and micro-porosity is considerably reduced, while the behaviour in the macro-porous region is not straightforward. The observed little shift towards higher pores, in macro-pores distribution is likely due to fissures and cracks generated during thermal treatment already

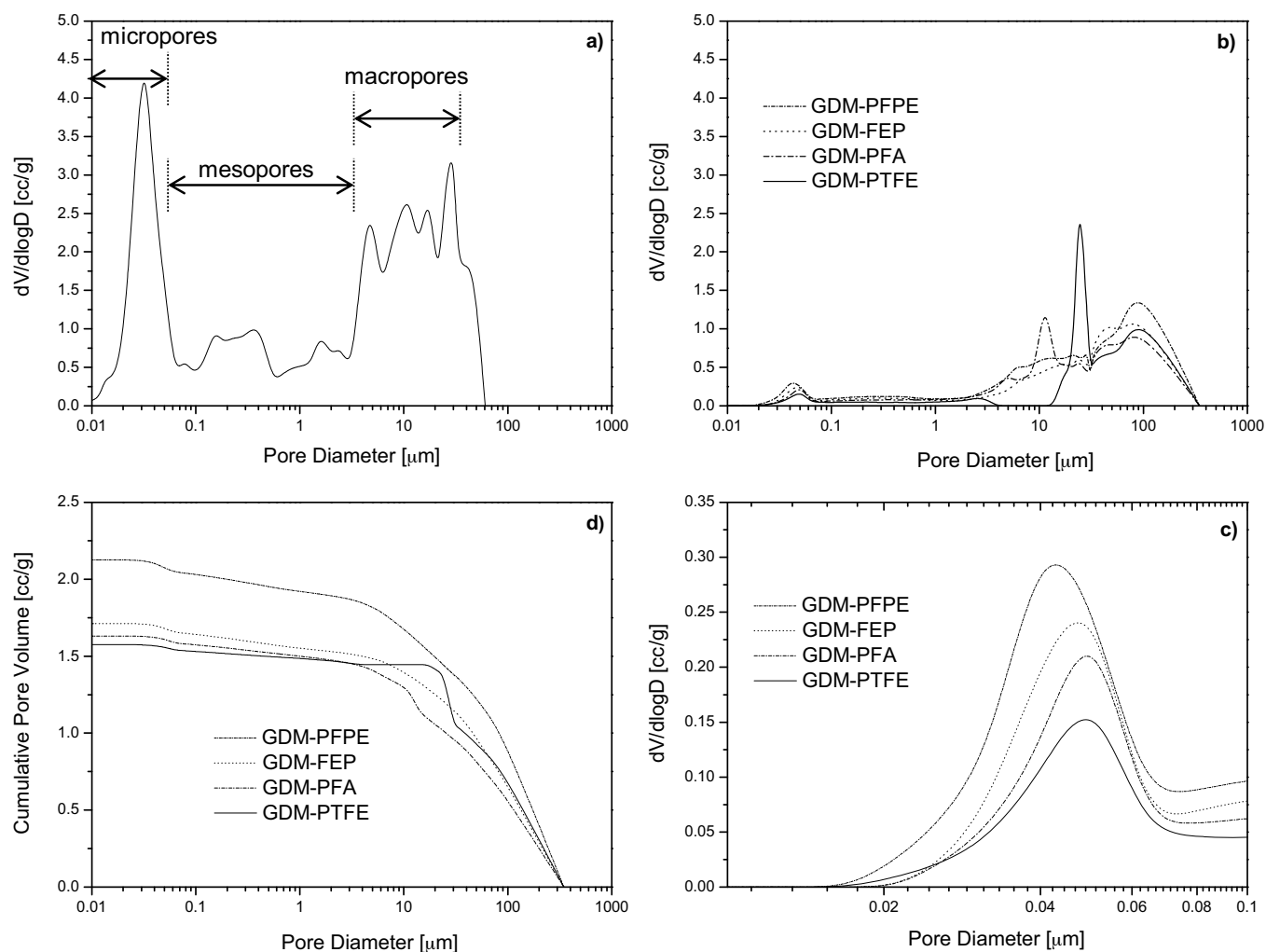


**Fig. 6.** Results of Hg porosimetry: pores size distribution for (a) carbon black and (b) GDMs, (c) off-set of the micro-porous region, (d) GDMs cumulative distribution.

discussed. The magnification of the micro-porous region (Fig. 6c) shows a dependence of the micro-pores distribution on the polymer nature: a progressive shift of the maximum towards lower pore diameters is found. A similar behaviour is found on cumulative pore volume (Fig. 6d); in particular, the higher is the melting temperature the lower is the volume. In fact, the PFPE-treated GDM, where polymer has no melting temperature, shows the highest cumulative pore volume among the four prepared samples suggesting that the original porosity cannot be modified because of the lack of polymer melt. On the contrary, in the other samples the melting process allows a more homogeneous distribution of the polymer, which, being liquid during thermal treatment, could cover the fibres and the carbon particles thus modifying, upon cooling, the original pores size and distribution, due to pores blocking. Mechanism and extent of the pores blocking is apparently independent on fluorinated polymer; indeed, the micro-pore diameters of the GDMs are all very similar, being in the range 0.043 and 0.05  $\mu\text{m}$  (Fig. 6c).

### 3.5. Contact angle

Fig. 7 reports (by a box-plot chart) the results of contact angle measurement on the investigated surfaces at 20 °C, 60 °C and 80 °C.

It can be noticed how all the surfaces are highly hydrophobic. Particularly, all samples apart from GDL treated with PTFE (GDL-PTFE) and GDL treated with PFPE (GDL-PFPE) exceed the limit of superhydrophobicity (contact angle higher than 150°), for all the

investigated temperatures. The GDL-PTFE and GDL-PFPE surfaces come close to superhydrophobicity at room temperature, while they become only hydrophobic when heated at 60 °C and 80 °C. The worsening of the hydrophobic behaviour is slightly larger for the GDL-PFPE sample.

At room temperature, contact angles in the range 155–162° can be found for the majority of the considered surfaces. On increasing the measurements temperatures, a general trend towards a slight reduction of the contact angle accompanied by a larger standard deviation is observed. However, such variation is nevertheless too low to be assumed, with statistical confidence, as a real difference of contact angle from sample to sample, also considering the measurement uncertainty.

In summary, it can be concluded that FEP and PFA surfaces show a very good hydrophobic behaviour when the polymer is used in both GDLs and GDMs. In the case of PTFE- and PFPE-treated surfaces GDLs more wettable than FEP and PFA are obtained, even though the subsequent deposition of the micro-porous layer is very effective in improving the hydrophobicity of the system to reach more or less the level of the other surfaces.

### 3.6. Electrochemical performances

Comparison of the electrical performances of the four GDMs when used in a lab-scale fuel cell was performed to find a possible composition–performances correlation.

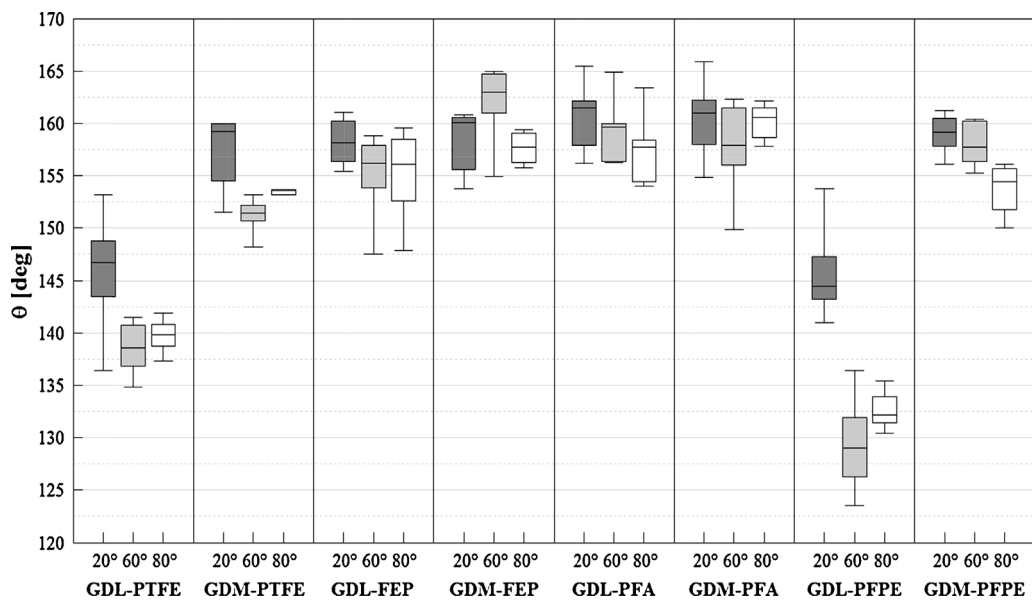


Fig. 7. Contact angle values on the investigated surfaces at 20 °C, 60 °C and 80 °C.

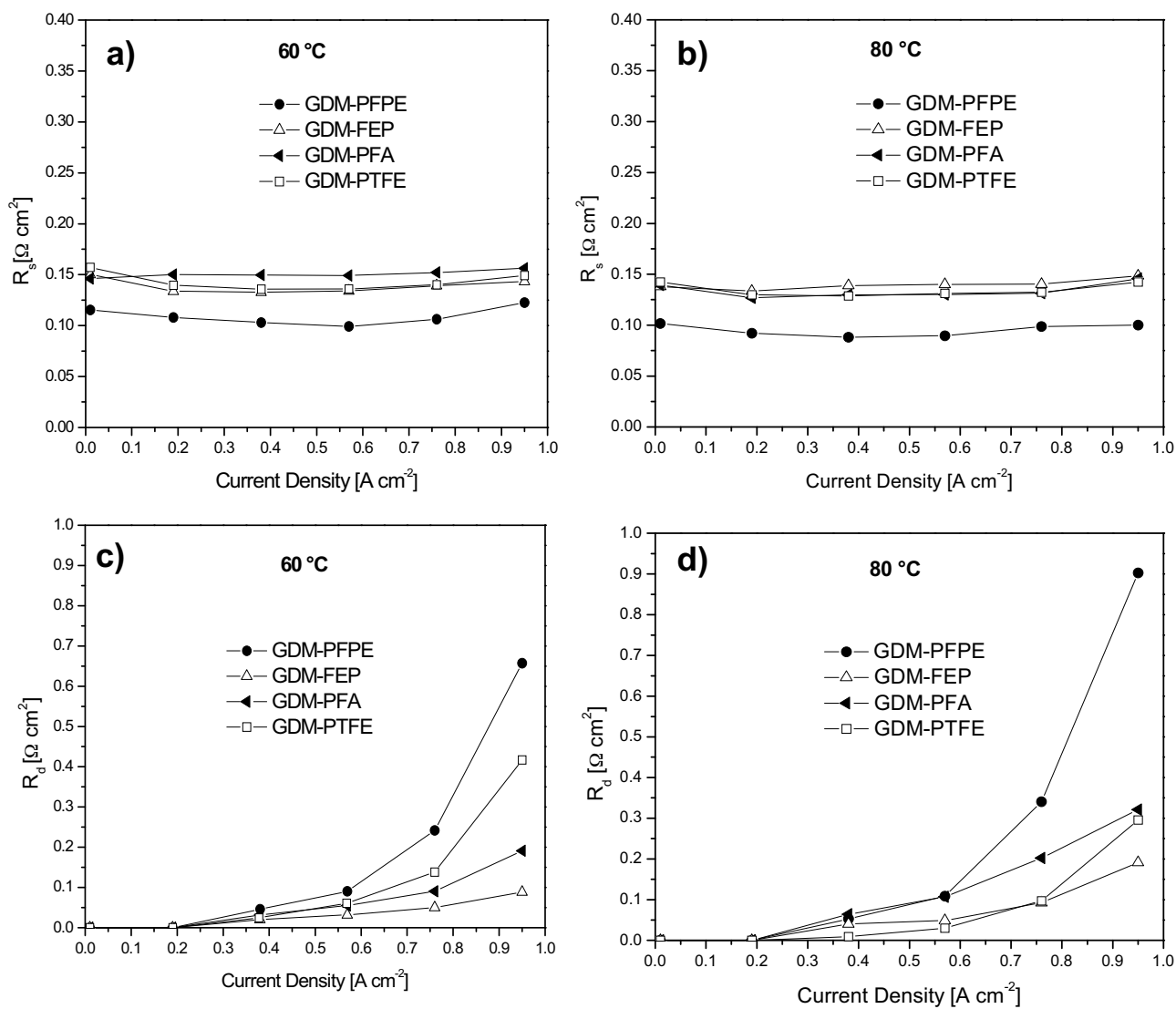


Fig. 8. Electrochemical parameters obtained from impedance spectroscopy of the running fuel cells assembled with the four GDMs: ohmic resistance at 60 °C (a) and 80 °C (b) and diffusion resistance at 60 °C (c) and 80 °C (d).

**Table 2**

Maximum output power density reached by fuel cells assembled with the different GDMs at 60 and 80 °C.

Sample	$P_{\max}$ (60 °C) (mW cm <sup>-2</sup> )	$P_{\max}$ (80 °C) (mW cm <sup>-2</sup> )
GDM-PFPE	448	450
GDM-FEP	519	458
GDM-PFA	457	436
GDM-PTFE	422	435

Fig. 8 shows the trends of the electrochemical parameters  $R_{\Omega}$  (ohmic resistance) and  $R_d$  (diffusion or mass transfer resistance) upon increasing current density, obtained from impedance spectroscopy at 60 and 80 °C on the running fuel cell assembled with the four GDMs. These parameters have been selected as more representative because influenced by composition and morphology of the GDM. The maximum power densities reached are summarized in Table 2 and they show how the new hydrophobic polymers, above all FEP, are effective in improving the global output performance of the fuel cell with respect to performance obtained using PTFE-based GDMs. In particular, the gain in performances is more evident at 60 °C, likely due to a change in surface energy and wettability of coatings upon increasing temperature from 60 to 80 °C, as contact angle measurements have evidenced (Fig. 7), although not sharply.

Ohmic resistance (Fig. 8a and b) does not vary significantly upon increasing current density, as expected and known [44]. However a small reduction in ohmic resistance is observed when temperature is increased from 60 to 80 °C due to a higher proton conductivity of the membrane, which influences the whole system resistance.

PFPE allows to reduce  $R_{\Omega}$  parameter, at both temperatures, but this better condition is not reached for  $R_d$ : GDM-PFPE shows the highest mass transfer resistances both at 60 and 80 °C (Fig. 8c and d), while FEP exhibits the best situation, namely very low  $R_d$  values.

Such a behaviour may be related to wettability of GDMs surfaces: FEP showed the highest contact angle values while PFPE the lowest ones among the innovative polymers employed. Moreover, PFPE-based GDM, even at the eye inspection (see SEM images), evidenced a bad adhesion of the MPL to GDL substrate. The lack in adhesion is reasonably ascribed to the lack of a melting process for this polymer. This could cause detachment of the micro-porous layer, which may drive to a worse water management, strictly related to values of  $R_d$ . Diffusion resistances increase upon increasing the water amount in fuel cell channels and only a hydrophobic (better if superhydrophobic) layer, such as GDMs based on FEP or PFA can eliminate excess water, avoiding flooding and improving the performance of the whole system.

#### 4. Conclusions

Gas diffusion medium was thought as a component for improving the contact between catalyst layer and bipolar plate leading to an increase of PEM fuel cell efficiency. Moreover it has to be hydrophobic in order to guarantee the fast removal of water produced by cathodic reduction reaction.

In this work, the hydrophobicity and electrochemical performances of the whole fuel cell system was assessed. Accordingly, three different kinds of inks for micro-porous layers deposition were prepared using PFPE, FEP and PFA as hydrophobic agents in order to replace conventional GDMs based on PTFE.

Rheological properties of inks were tested and they were found comparable with conventional PTFE-based inks: shear thinning fluids, which are of choice for applying the blade coating technique, were obtained. A good stability and reproducibility of the inks were also obtained.

Coating thicknesses similar to that one of PTFE-based MPL were found, upon proper tuning of the deposition rate as function of the

different viscosities obtained with the PFPE, FEP- and PFA-based inks.

Upon thermal treatment, a reasonable homogeneity of GDMs was achieved. Except for GDM-PFPE, also a good adhesion of the micro-porous layers to the GDL substrate has been observed. The worse adhesion of PFPE-based MPL can be ascribed to the absence of melting point in this polymer. For the other samples, despite cracks formation, no manifest detachment of the coated layer was found.

Superhydrophobicity seems to be the parameter of selection to modify the fuel cell behaviour during operation. FEP-containing GDMs showed a superhydrophobic surface that allowed to reduce significantly mass transfer limitations both at 60 and 80 °C, and the fuel cell assembled with such GDMs reached the highest power density. Thus, FEP could really be considered as a reasonable alternative to PTFE in GDMs fabrication.

#### Acknowledgments

Authors gratefully thank Dr. Leonardo Giani for technical support about fluorinated polymers and Dr. Renato Pelosato for his help in performing and discussing XRD measurements.

#### References

- [1] C. Stone, *Solid State Ionics* 152 (2002) 1–13.
- [2] M.L. Perry, T.F. Fuller, *J. Electrochem. Soc.* 149 (2002) S59–S67.
- [3] J. Wee, *Renew. Sustain. Energy Rev.* 11 (2007) 1720–1738.
- [4] F. Barbir, *PEM Fuel Cells: Theory and Practice*, Elsevier Academic Press, Oxford, UK, 2005.
- [5] L. Venturelli, P.E. Santangelo, P. Tartarini, *Appl. Therm. Eng.* 29 (2009) 3469–3475.
- [6] U.H. Jung, S.U. Jeong, K.T. Park, H.M. Lee, K. Chun, D.W. Choi, S.H. Kim, *Int. J. Hydrogen Energy* 32 (2007) 4459–4465.
- [7] J. Chen, T. Matsuura, M. Hori, *J. Power Sources* 131 (2004) 155–161.
- [8] G.G. Park, Y.J. Sohn, T.H. Yang, Y.G. Yoon, W.Y. Lee, C.S. Kim, *J. Power Sources* 131 (2004) 182–187.
- [9] G. Unsworth, N. Zamel, X.G. Li, *Int. J. Hydrogen Energy* 37 (2012) 5161–5169.
- [10] H.Y. Lee, J.Y. Kim, J.H. Park, Y.G. Joe, T.H. Lee, *J. Power Sources* 131 (2004) 188–193.
- [11] S. Park, J.W. Lee, B.N. Popov, *Int. J. Hydrogen Energy* 37 (2012) 5850–5865.
- [12] T. Kitahara, T. Konomi, H. Nakajima, *J. Power Sources* 195 (2010) 2202–2211.
- [13] S. Latorrata, P.G. Stampino, E. Amici, R. Pelosato, C. Cristiani, G. Dotelli, *Solid State Ionics* 216 (2012) 73–77.
- [14] T. Kitahara, H. Nakajima, K. Mori, *J. Power Sources* 199 (2012) 29–36.
- [15] S.G. Kandlikar, M.L. Garofalo, Z. Lu, *Fuel Cells* 11 (2011) 814–823.
- [16] M.V. Williams, E. Begg, L. Bonville, H.R. Kunz, J.M. Fenton, *J. Electrochem. Soc.* 151 (2004) A1173–A1180.
- [17] T. Tanuma, S. Kinoshita, *J. Electrochem. Soc.* 159 (2012) B150–B154.
- [18] T.L. Liu, C. Pan, *J. Power Sources* 207 (2012) 60–69.
- [19] U. Pasaogullari, C.Y. Wang, *J. Electrochem. Soc.* 151 (2004) A399–A406.
- [20] A.Z. Weber, J. Newman, *J. Electrochem. Soc.* 152 (2005) A677–A688.
- [21] S. Park, B.N. Popov, *Electrochim. Acta* 54 (2009) 3473–3479.
- [22] C. Lim, C.Y. Wang, *Electrochim. Acta* 49 (2004) 4149–4156.
- [23] R.L. Borup, J.R. Davey, F.H. Garzon, D.L. Wood, M.A. Inbody, *J. Power Sources* 163 (2006) 76–81.
- [24] Y. Yuan, I. Cabasso, X. Xu, *Gas Diffusion Electrodes Based on Poly(vinylidene fluoride) Carbon Blends*, US Patent No. 5783325 (1998).
- [25] W.M. Yan, D.K. Wu, X.D. Wang, A.L. Ong, D.J. Lee, A. Su, *J. Power Sources* 195 (2010) 5731–5734.
- [26] S.B. Park, Y.I. Park, *Int. J. Precis. Eng. Manuf.* 13 (2012) 1145–1151.
- [27] W.W. Purwanto, V.J. Slamet, B. Wargadalam, Pranoto, *Int. J. Electrochem. Soc.* 7 (2012) 525–533.
- [28] P.G. Stampino, S. Latorrata, D. Molina, S. Turri, M. Levi, G. Dotelli, *Solid State Ionics* 216 (2012) 100–104.
- [29] M. Licchelli, S.J. Marzolla, A. Poggi, C. Zanchi, *J. Cult. Herit.* 12 (2011) 34–43.
- [30] M. Jiang, X.L. Zhao, X.B. Ding, Z.H. Zheng, Y.X. Peng, *Eur. Polym. J.* 41 (2005) 1798–1803.
- [31] N. Stobie, B. Duffey, S.J. Hinder, P. McHale, D.E. McCormack, *Colloids Surf. B* 72 (2009) 62–67.
- [32] T. Trombetta, P. Iengo, S. Turri, *J. Appl. Polym. Sci.* 98 (2005) 1364–1372.
- [33] B. Jones, *JCT CoatingsTech* 5 (2008) 44–48.
- [34] C.S. Kong, D.Y. Kim, H.K. Lee, Y.G. Shul, T.H. Lee, *J. Power Sources* 108 (2002) 185–191.
- [35] O.I. del Rio, A.W. Neumann, *J. Colloid Interface Sci.* 196 (1997) 136–147.
- [36] R. Tadmor, P.S. Yadav, *J. Colloid Interface Sci.* 317 (2008) 241–246.
- [37] M. Guizzoni, *J. Colloid Interface Sci.* 364 (2011) 230–236.



- [38] M. Santini, M. Guilizzoni, S. Fest-Santini, J. Colloid Interface Sci. 409 (2013) 204–210.
- [39] G.L. Mack, D.A. Lee, J. Phys. Chem. 40 (1936) 169–176.
- [40] A.A. Tracton, Coatings Materials and Surface Coatings, CRC Press, Boca Raton, FL, 2007.
- [41] J.F. Lin, X. Liu, A. Adame, R. Villacorta, J. Wertz, R. Ahmad, M. Thommes, A.M. Kannan, Electrochim. Acta 56 (2011) 1591–1596.
- [42] J.H. Nam, M. Kaviany, Int. J. Heat Mass Transfer 46 (2003) 4595–4611.
- [43] L. Cindrella, A.M. Kannan, J.F. Lin, K. Saminathan, Y. Ho, C.W. Lin, J. Wertz, J. Power Sources 194 (2009) 146–160.
- [44] L. Omati, P.G. Stampino, G. Dotelli, D. Brivio, P. Grassini, Int. J. Hydrogen Energy 36 (2011) 8053–8062.